AD-A120 386 SPECTROSCOPY RELAXATION AND EXCITATION TRANSFER OF OPTICALLY EXCITED STATES IN SOLIDS(U) COLUMBIA UNIV NEW YORK DEPT OF PHYSICS S R HARTMANN OCT 82 1/1

UNCLASSIFIED ARO-17379.2-PH NSF-DMR80-06966 F/G 20/10 NL

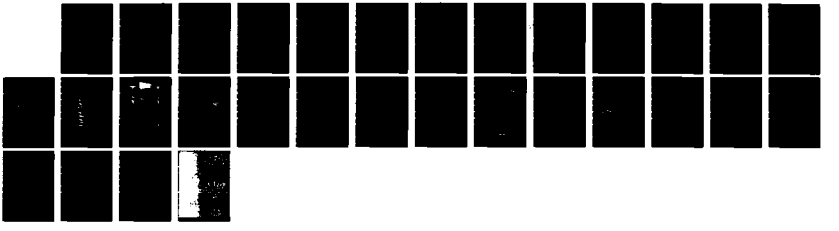

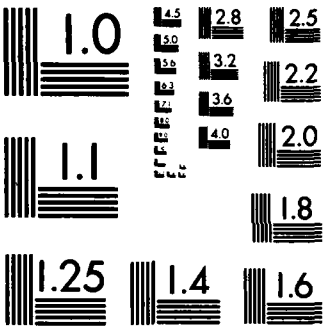

REPORT DOCUMENTATION PAGE

READ INSTRUCTIONS BEFORE COMPLETING FORM

1. REPORT NUMBER: 17379.2-PH	2. GOVT ACCESSION NO.
3. RECIPIENT'S CATALOG NUMBER	
4. TITLE (and Subtitle): Spectroscopy, Relaxation, and Excitation Transfer of Optically Excited States in Solids	5. TYPE OF REPORT & PERIOD COVERED: Final: 1 Aug 80 - 31 Jul 82
6. PERFORMING ORG. REPORT NUMBER	
7. AUTHOR(s): Sven R. Hartmann	8. CONTRACT OR GRANT NUMBER(s): ARO 40-80; 40-81
9. PERFORMING ORGANIZATION NAME AND ADDRESS: Columbia University, New York, NY 10027	10. PROGRAM ELEMENT, PROJECT, TASK AREA & WORK UNIT NUMBERS
11. CONTROLLING OFFICE NAME AND ADDRESS: U. S. Army Research Office, Post Office Box 12211, Research Triangle Park, NC 27709	12. REPORT DATE: Oct 82
	13. NUMBER OF PAGES: 27
14. MONITORING AGENCY NAME & ADDRESS(if different from Controlling Office)	15. SECURITY CLASS. (of this report): Unclassified
	15a. DECLASSIFICATION/DOWNGRADING SCHEDULE

16. DISTRIBUTION STATEMENT (of this Report)

Approved for public release; distribution unlimited.

17. DISTRIBUTION STATEMENT (of the abstract entered in Block 20, if different from Report)

NA

18. SUPPLEMENTARY NOTES

The view, opinions, and/or findings contained in this report are those of the author(s) and should not be construed as an official Department of the Army position, policy, or decision, unless so designated by other documentation.

19. KEY WORDS (Continue on reverse side if necessary and identify by block number)

20. ABSTRACT (Continue on reverse side if necessary and identify by block number)

The central focus of the research performed under this contract involved the optical $^3H_4$ - $^1D_2$ transition of the Pr^{3+} ion in LaF_3. In addition to this transition, a theoretical analysis of propagation narrowing in the transmission of a light pulse through a spectral hole was performed.

DD FORM 1 JAN 73 1473 EDITION OF 1 NOV 65 IS OBSOLETE

FINAL REPORT

(TWENTY COPIES REQUIRED)

1. ARO PROPOSAL NUMBER: 17379-P

2. PERIOD COVERED BY REPORT: August 1, 1980 - July 31, 1982

3. TITLE OF PROPOSAL: Spectroscopy, Relaxation, and Excitation Transfer of Optically Excited States in Solids

4. CONTRACT OR GRANT NUMBER: NSF-DMR80-06966

5. NAME OF INSTITUTION: Columbia University

6. AUTHOR(S) OF REPORT: Professor Sven R. Hartmann

7. LIST OF MANUSCRIPTS SUBMITTED OR PUBLISHED UNDER ARO SPONSORSHIP DURING THIS PERIOD, INCLUDING JOURNAL REFERENCES:

K. Chiang, E.A. Whittaker, and S.R. Hartmann, "Photon Echo Nuclear Double Resonance in $LaF_3:Pr^{3+}$" Phys. Rev. B 23, 6142 (1981).

J.H. Eberly, S.R. Hartmann, and A. Szabo, "Propagation Narrowing in the Transmission of a Light Pulse through a Spectra Hole," Phys. Rev. A 23, 2502 (1981).

E. Whittaker and S.R. Hartmann, "Photon Echo Modulation between the $^3H_4$ - $^1D_2$ Levels of $Pr^{3+}:LaF_3$," Accepted to XIIth IQEC.

*E.A. Whittaker and S.R. Hartmann, "Hyperfine Structure of the $^1D_2$ - $^3H_4$ Levels of $Pr^{3+}:LaF_3$ with the use of Photon Echo Modulation Spectroscopy, Phys. Rev. B 26, xxx (1982).

8. SCIENTIFIC PERSONNEL SUPPORTED BY THE PROJECT AND DEGREES AWARDED DURING THIS REPORTING PERIOD:

S. R. Hartmann, Professor of Physics
T. W. Mossberg, Assistant Professor of Physics
E. A. Whittaker, Graduate Research Assistant (Degree Awarded 1982)
R. Kichinski, Graduate Research Assistant

Dr. S. R. Hartmann 17379-P
Columbia University
Columbia Radiation Laboratory
Department of Physics
New York, NY 10027

*During January 1, 1982 - July 31, 1982

BRIEF OUTLINE OF RESEARCH FINDINGS

The central focus of the research performed under this contract involved the optical $^3H_4 - {}^1D_2$ transition of the Pr^{3+} ion in LaF_3. Our plan was to perform a photon echo modulation experiment similar to the one used to study the optical $^3H_4 - {}^3P_0$ transition of the Pr^{3+} ion in LaF_3.[1] (In that experiment modulation data provided ground and excited state spectroscopic information, nuclear hyperfine linewidths, the optical homogeneous linewidth and the relative orientation of the principle axes of the ground and excited state hyperfine hamiltonians.

The Pr^{3+} ion in crystals of LaF_3 substitutes for the La atom and exhibits an absorption and emission spectrum characteristic of an ion whose energy levels are nondegenerate.[2] Although the crystal structure of LaF_3 is somewhat controversial, the most likely model appears to be that proposed by Mansmann[3] and Zalkin et al.[4] They suggest P3c1 - D^3_{3d} which has a trigonal structure with six molecules per unit cell and which exhibits C_2 point symmetry about each of the three inequivalent La sites. The twofold axis of C_2 is normal to the crystal c axis. Since the Pr^{3+} ion has two unpaired 4f electrons, the low symmetry at the La site removes all the degeneracy of the energy eigenstates and requires that for each eigenstate $\langle \vec{J} \rangle = \vec{0}$ where J is the electronic angular momentum operator. To first order then, the Pr^{3+} ions have no electronic magnetism and one might expect that they would be well isolated. It follows that in any coherent optical transient experiment they should behave in a simple manner. It is not surprising then that Takeuchi and Szabo[5] found that, in contrast to the case of ruby,[6] it is possible to observe photon echoes in LaF_3:Pr^{3+} without the application of an external magnetic field. They worked in the $^3H_4 - {}^3P_0$ transtiion (4777Å) at liquid

helium temperatures. The echoes appeared to decay exponentially with pulse separation τ.

The first observation of a nonexponential decay for the echo intensity versus τ in $LaF_3:Pr^{3+}$ was reported by Chen et al.[7] who found a sharp rephasing at $\tau \cong 240$ nsec, just beyond the region studied by Takeuchi.[5] They also reported the observation of echoes in the $^1D_2 - {}^3H_4$ transition (5925 Å) which were modulated at the inverse of 8.47 MHz, the $^3H_4$ ground-state splitting frequency. More recent experiments by Chen et al.[8] and Morsink and Wiersma[9] using independently triggered nitrogen-pumped dye lasers have confirmed the observed rephasing at 240 nsec and have shown that the echo-decay envelope is more complex than had previously been expected. This complexity is fortunate however as it allows analysis to discover the most complete description of the Pr^{3+} ion with its environment.

Our first work on the $^3H_4 - {}^1D_2$ transition encountered difficulty because of the relatively weak character of the transition dipole moment. Experimental difficulty aside we were able to obtain echo modulation data but we were unable to analyze it successfully. Two problems were encountered. First the best theoretical fit we could obtain to the modulation data was not very satisfying and this fit required that we discount Erickson's[10,11] measurements of the $^1D_2$ state splitting. On re-analyzing Erickson's work we felt (as did Erickson in a private conversation) that for the $^1D_2$ state the results were not unambiguous and a more direct measurement of the excited state splitting was in order. In Erickson's experiment he "sees" many resonances and these must be carefully handled to achieve the desired result. There was also the surprising circumstance that his inferred excited state splittings of 3.7 MHz and 4.7 MHz summed too close to the 8.48 MHz splitting of two of the ground state levels. This coincidence was disturbing to both Erickson and us. We therefore proceeded to make a direct measurement of the

terminal level splittings by the PENDOR technique. This method was developed in our laboratory and was successfully used to obtain the hyperfine interactions between the Cr^{3+} ion and the neighboring Al nuclei in ruby ($Cr^{3+}:Al_2O_3$). The method has the advantage that its results are unambiguous. It works by exploiting the dependence of the three-pulse stimulated photon echo amplitude on the application of an rf field which is resonant with a hyperfine transition. We performed such an experiment and found Erickson's work to be wholly correct. This work was published in Physical Review and appears herein as Appendix A.

Our difficulty in analysing our photon echo modulation data was traced to the existence of a long-lived stimulated echo which constructively interfered with our two-pulse photon echo. In our experiment, the ordinary two pulse echo, needed to gather the modulation data, is formed by a pair of pulses, separated in time by 0.1 microseconds to 9 microseconds. The effect of the two pulses is to produce the ordinary photon echo delayed from the second pulse by the pulse separation. The pulse pair also induces order in the population distribution of the ground state hyperfine levels (optical pumping) and due to the very long spin lattice relaxation time of the system,[12] the order will persist for as long as several minutes. A laser pulse applied to such an ordered system will generate a stimulated echo, delayed in time from the pulse by the same amount as the pulse separation between the pair of pulses which induced the order in the first place. In our usual data taking method, pairs of pulses arrive at the sample at the repetition frequency of the laser (10 Hz.), forming a complicated sequence of echoes and stimulated echoes simultaneously. To eliminate this problem we applied radio-frequency energy at one of the ground state hyperfine resonances (16.7 MHz) during the interval between laser shots, effectively eliminating the population distribution order and the long-lived stimulated

echo.

Eliminating the stimulated echo removed the major obstacle in the way of obtaining reliable modulation data. The other major problem area was signal to noise. Echo modulation experiments require signal handling with a wide dynamic range. We were ultimately able to see echoes over a range of 10^4 but that was only possible through hard work. Narrowing the spectral width of our laser to 4 GHz helped as well as going to samples whose resonances were just on the verge of being optically thick. We improved our computer assisted data taking process. In particular, two new computer operated peripherals were installed in the system. The first is a computer controllable electrical attenuator which is used to maintain the modulated signal within the linear range of the data acquisition electronics. The computer is thus able to adjust the signal level automatically. The second device is a pair of digitally programmable pulse generators, used to set the laser pulse separation and Pockel's cell gate. These devices are of a "random access" nature allowing the pulse separation to be varied over several orders of magnitude between a single laser shot. This allows us to periodically measure the echo magnitude at a single fixed reference time without suffering a loss in the data taking rate. The reference measurement allows us to compensate for echo amplitude drift during the course of a single data taking run, as well as providing a normalization factor which facilitates averaging data sets from different runs.

With the improvements in the technique outlined above we have been able to obtain excellent echo modulation data with which to analyze the $^3H_4 - {}^1D_2$ transition of Pr^{3+} in LaF_3. The analysis involves both Fourier analysis to yield spectroscopic information directly and theoretical echo modulation reconstruction to provide the detailed form of the interaction hamiltonian. This work will be published in Physical Review and a proof of the article

appears in Appendix B.

The resonance widths of $Pr^{3+}:LaF_3$ reflect the total (inhomogeneous and homogeneous) nuclear linewidths of the various hyperfine transitions. Previous measurements[1,13] have shown the ground state widths to be about 200 kHz. This width is mostly inhomogeneous and arises from the interaction of the enhanced ground state ^{141}Pr nuclear moment of 11.5 kHz/G with the surrounding distribution of static ^{19}F nuclear moments. Macfarlane and Shelby[13] have measured the g-tensor for the $^1D_2$ state and found the enhancement to be roughly one-fifth as much as in the ground state. This would lead one to expect a much narrower linewidth for the nuclear transitions in the $^1D_2$ state and our measurement, while very nearly resolution-limited by the overall echo decay envelope, establishes a new upper limit of 30 kHz [FWHM] for the hyperfine line at 8.51 Mhz, consistent with this expectation. The linewidths of the hyperfine at 3.72 and 4.79 MHz are somewhat larger, being 70 kHz, and 60 kHz respectively. The results for the $^1D_2$ excited state parameters are summarized in Table 1.

The effective hyperfine Hamiltonian is given by

$$H_{g(e)} = P_{g(e)}[I^2_{z(Z)} + \frac{\eta_{g(e)}}{3}(I^2_{x(X)} - I^2_{y(Y)}] \qquad (1)$$

where $P_{g(e)}$ and $\eta_{g(e)}$ are interaction constants. The upper and lower case subscripts emphasize that the ground (g) and excited (e) state principal axes need not be the same, although Neumann's principle requires that they have at least one common axis parallel to the local C_2 symmetry axis. This constraint significantly reduces the number of possible orientations and we may represent these possibilities on a two-dimensional map. The coordinates of such a map give the particular choice of common axis, and the angle θ through which one set of axes is rotated with respect to the other set about

the common axis. Since the Hamiltonian in Eq. 1 is insensitive to the sign of the coordinates an orientation of, say, $\hat{x} \parallel \hat{X}$ is equivalent to $\hat{x} \parallel -\hat{X}$. We have calculated the echo modulation in increments of five degrees in the rotation angle θ. In the map presented in Fig. 1, for each orientation coordinate a box is drawn whose width is proportional to the minimum mean square deviation between our data and the calculated modulation. Only the first microsecond of data were used in the fitting procedure for Figure 1. Beyond one μsec. the data are dominated by the excited state hyperfine splittings, due to the relative linewidths of ground and excited state levels, and including these data in the fit considerably reduces the selectivity of the map.

Figure 2 shows in expanded scale the first three μsec of the data, and Figure 3 shows the theoretical curve that was calculated using the orientation coordinate giving the best fit to the data (as indicated by an arrow in the lower left of Figure 1).

The map in Figure 1 shows a high degree of symmetry and concommitant lack of selectivity for determining the orientation parameter. To explore the extent to which this symmetry is intrinsic, we have substituted for the data used to calculate the map of Figure 1 the values of the theoretical modulation corresponding to Figure 3, producing the map shown in Figure 4. The scale in Figure 4 was chosen to make the box corresponding to the coordinate with the worst fit in Figure 4 approximately the same size as the box with the worst fit in Figure 2. It is apparent that the high degree of symmetry persists. To estimate the extent to which our signal-to-noise would have to improve to allow us to select one orientation with certainty, we replotted Figure 4 with the box width scale expanded by a factor of ten, as shown in Figure 5. It appears that an improvement in signal-to-noise by a factor of ten or twenty would have made possible a more definitive statement

about the orientation. This improvement will probably come from the use of frequency and amplitude stabilized dye lasers. Frequency jitter in particular causes considerable fluctuation in echo intensity, presently averaged by the data-taking system, and such averaging tends to wash out some of the fine details of the modulation pattern. Despite the high symmetry, we can draw a number of conclusions about the relative orientation. All configurations with all axes parallel are ruled out, as are those with the excited state Z-axis parallel to C_2. These conclusions are similar to the measurement of Chen et al.,[1] on the relative orientation of the $^3H_4$ and $^3P_0$ states. Since the g-tensor is nearly isotropic in the $^1D_2$ state[13] and absent completely in the $^3P_0$ state the relative orientation parameter must be primarily determined by the relative orientation of the pure quadrupole tensor with respect to the ground state hyperfine tensor.

In addition to the study of the $^3H_4$ - $^1D_2$ Pr^{3+} transition we also performed a theoretical analysis of propagation narrowing in the transmission of a light pulse through a spectral hole. This work appeared in Physical Review and is attached as Appendix C. Because of the linearity of the system, it is possible to treat the pulse as if it were interacting with two entirely separate groups of atoms. The first group comprises the usual dipole oscillators in the full Doppler line, and the second group is a set of "negative" oscillators in a narrow region which serve to "eat out" the hole. The negative oscillators emit rather than absorb light. It is the emission of the "negative" oscillators that cause narrowing of the transmitted pulse spectrum as obtained by our theoretical analysis.

References

1. Y. C. Chen, K. Chiang, and S. R. Hartmann, Phys. Rev. B 21, 40 (1980).

2. W. M. Yen, W. C. Scott, and a. L. Schawlow, Phys. Rev. A 136, 271 (1964).

3. Von M. Mansmann, z. anorg, allg. Chem. 331, 98 (1964).

4. A. Zalkin, D. H. Templeton, and T. E. Hoplins, Inorg. Chem. 5, 1466 (1966).

5. N. Takeuchi and a. Szabo, Phys. Lett. A 50, 316 (1974).

6. N. A. Kurnit, I. D. Abella, and S. R. Hartmann, Phys. Rev. Lett. 13, 567 (1976).

7. Y. C. Chen, K. Chiang, and S. R. Hartmann, Opt. commun. 26, 269 (1978).

8. T. C. Chen, K. C. Chiang, and S. R. Hartmann, Opt. Commun. 29, 181 (1979).

9. J. B. W. Morsink and D. A. Wiersma, Chem. Phys. Lett. 65, 109 (1979).

10. L. E. Erickson, Opt. commun. 21, 147 (1977).

11. L. E. Erickson, Phys. Rev. B 16, 4731 (1977).

12. R. M. Shelby, R. M. Macfarlane, and C. S. Yannoni, Phys. Rev. B 21, 5004 (1980).

13. R. M. Macfarlane and R. M. Shelby, Opt. Lett. 6, 96 (1981).

Table 1

Resonance	Frequency	Full width at half max
ω_1^e	3.72 ± 0.02 MHz	70 ± 20 kHz
ω_2^e	4.79 ± 0.02 MHz	60 ± 20 kHz
ω_{12}^e	8.51 ± 0.02 MHz	30 ± 30 kHz

Table 1: Values for the $^1D_2$ excited state hyperfine frequencies and nuclear linewidths obtained from the Fourier transform of the data. The linewidths have been corrected for the effect of the finite truncation interval.

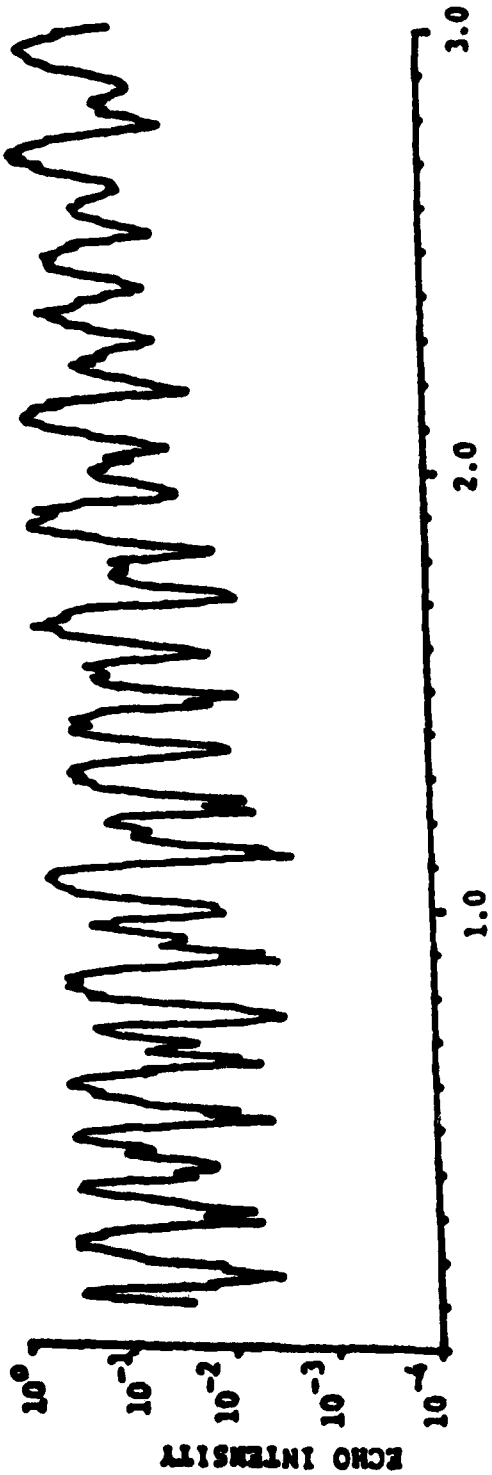

Figure 2. Echo intensities for pulse separations up to 3 μsec.

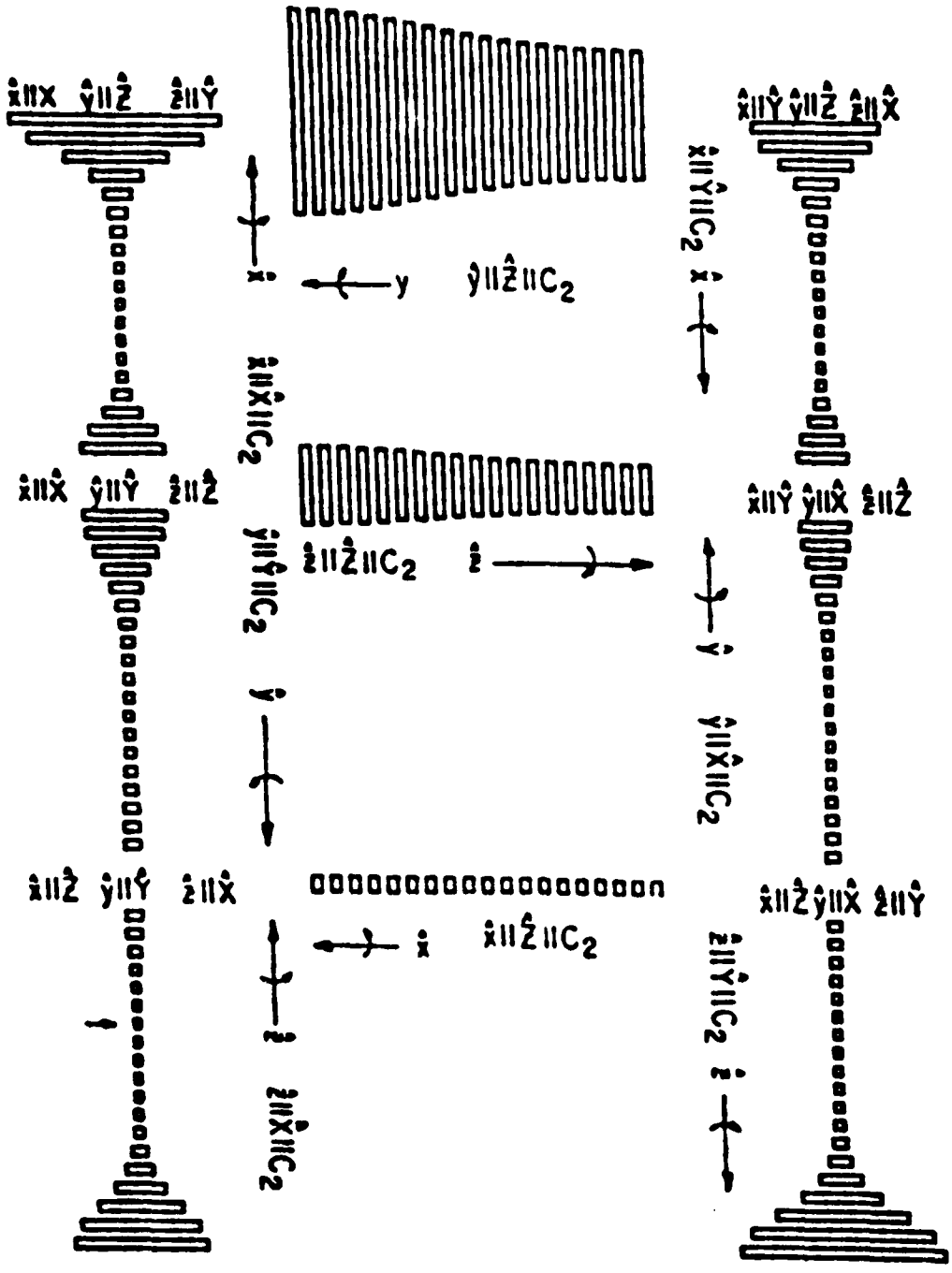
x
y
z
$\hat{y}\|\hat{z}\|C_2$
$\hat{x}\|\hat{Y}\|C_2$
$\hat{x}\|\hat{X}\|C_2$
$\hat{z}\|\hat{Z}\|C_2$
$\hat{y}\|\hat{X}\|C_2$
$\hat{x}\|\hat{Z}\|C_2$
$\hat{z}\|\hat{Y}\|C_2$
$\hat{z}\|\hat{X}\|C_2$

Figure 1.

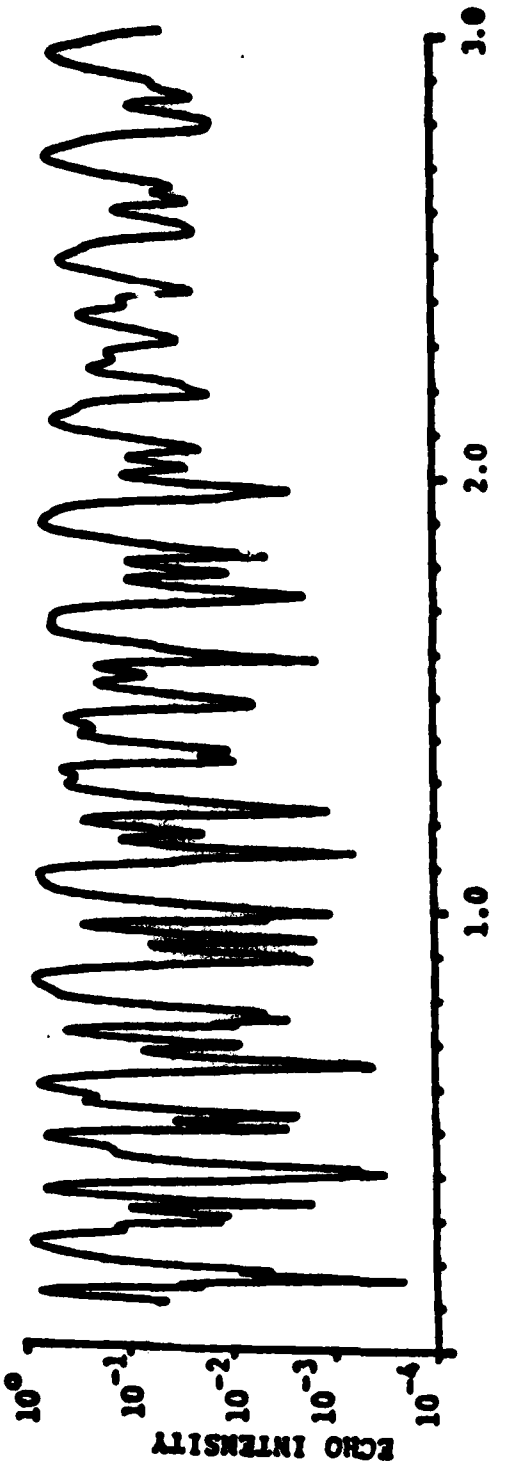

Figure 3. Theoretical dependence at echo intensity on pulse separation for the orientation coordinate giving the best fit to the data (as indicated by the arrow in Fig. 1).

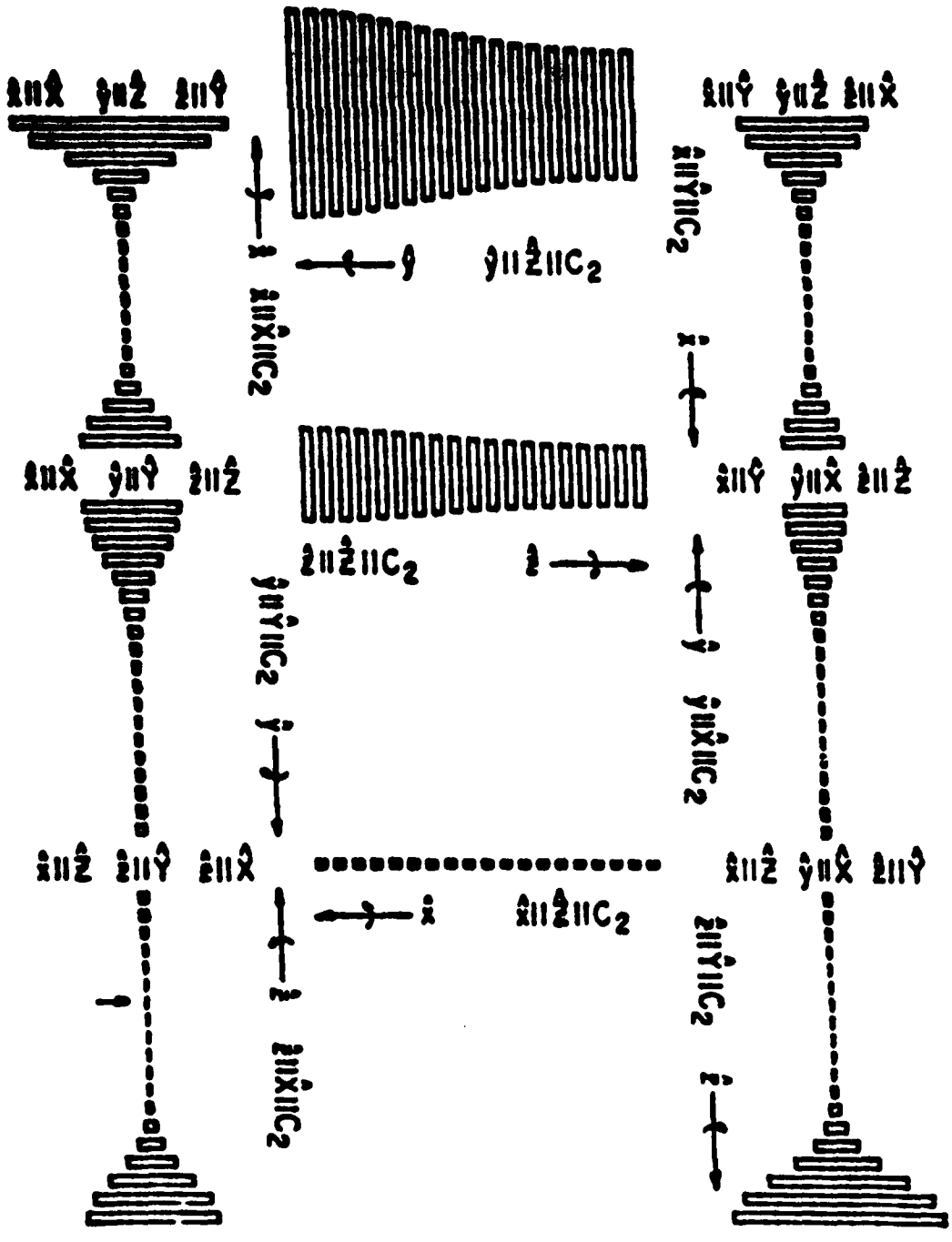

Figure 4. Map of mean square deviation between the theoretically calculated data of Figure 3 and the theoretical curve of Equation 1. Notice the similarity to Figure 1.

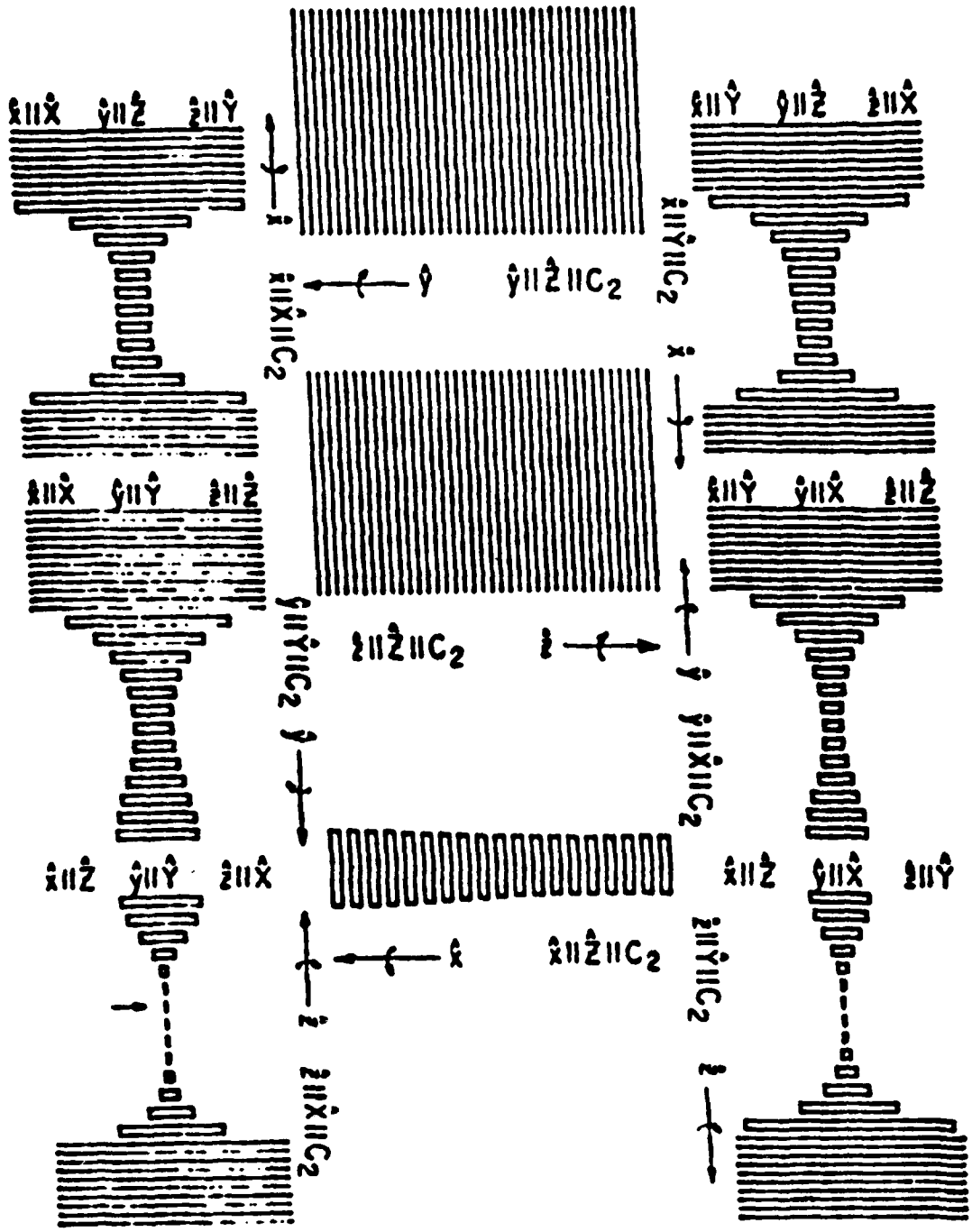

Figure 5. Map of Figure 4 with the scale for the box width expanded by a factor of ten.

Photon-echo nuclear double resonance in $LaF_3:Pr^{3+}$

K. Chiang,* E. A. Whittaker, and S. R. Hartmann
Columbia Radiation Laboratory, Department of Physics, Columbia University, New York, New York 10027
(Received 14 November 1980)

Using the photon-echo-nuclear-double-resonance technique, we have measured the nuclear hyperfine splittings in the excited $^1D_2$ state of $LaF_3:Pr^{3+}$. Our measurements are in agreement with the results obtained by Erickson from his saturated-and-enhanced-absorption study of the $^3H_4$-$^1D_2$ transition in $LaF_3:Pr^{3+}$.

Photon-echo modulation in $LaF_3:Pr^{3+}$ has been a valuable source for obtaining the various spectroscopic and relaxation parameters associated with the $^3H_4$-$^3P_0$ transition.[1] This technique when applied to the $^3H_4$-$^1D_2$ transition, however, has only had modest success.[2] In particular, echo modulation data taken in the standard manner are not altogether consistent[3] with the measured excited-state splittings as obtained by Erickson.[4,5] It was therefore felt that an independent measurement of the $^1D_2$ excited-state splittings was necessary to build confidence in their accuracy. To this end we have performed a photon-echo-nuclear-double-resonance (PENDOR) experiment[6] on the $^3H_4$-$^1D_2$ transition of this system.

The PENDOR technique was first applied to the measurement of energy splittings of ^{13}Al nuclei in a single crystal of ruby, and was used to obtain the interaction parameters of the Cr^{3+} ion with its surrounding nuclear neighbors in both the ground $^2A_4$ and excited $^2E(\bar{E})$ states of ruby.[7] Until our use of this technique to measure nuclear hyperfine splittings in $LaF_3:Pr^{3+}$, PENDOR had not been applied to the study of any material other than ruby.

A PENDOR experiment may be summarized as follows: Three laser pulses of resonant radiation are made incident on a sample to produce a stimulated photon echo, with a pulsed rf field applied to the sample during the interval between the second and third pulses. When the rf field is resonant with a nuclear transition in either of the two terminal levels of the echo transition, there will be a degradation of the echo intensity. This decrease in echo size is the double resonance signal. As is generally true in optical-rf double-resonance experiments, one obtains a sensitivity greatly increased over purely NMR or optical methods for several reasons. With PENDOR, the resolution is limited not by the linewidth of the laser used, as was the case in Erickson's enhanced-and-saturated-absorption method,[4] but only by the length of time over which the rf field is applied to the sample. Secondly, there are no ambiguities in the interpretation of the observed line shape. For example, in order to obtain the true inhomogeneous line shape of the nuclear transitions in the $^1D_2$ state in $LaF_3:Pr^{3+}$, Erickson had to deconvolve the measured line shape from the linewidth of the laser that he used. The inferred linewidths are quite sensitive to whether the measured line shape is assumed to be Gaussian or Lorentzian. A third and important advantage of PENDOR is that it can be used to study nuclear hyperfine structure in excited states of ions in solids that are not accessible to cw dye lasers because of power or spectral range considerations.

Stimulated photon echoes were produced on the transition (592.5 nm) connecting the lowest levels of the crystal-field-split components of the $^3H_4$ and $^1D_2$ states. These levels are electronic singlets that are further split into three doubly degenerate nuclear levels by the combined influence of the Pr^{3+} nuclear quadrupolar and second-order magnetic hyperfine dipolar interactions. The previously measured[1,4] nuclear splittings for both the $^3H_4$ and $^1D_2$ states are small compared to the 10-GHz bandwidth of the laser excitation pulses. The timing sequence for a PENDOR experiment is shown in Fig. 1.

Our experimental setup utilized two independently triggered nitrogen-laser-pumped dye lasers, which produce multiple-kW, 5-nsec-long pulses in a bandwidth of approximately 10 GHz. The output of one of the lasers was divided into two beams of roughly equal intensity by beam splitter BS (see Fig. 2). One beam was steered into an optical delay line (consisting of a White cell with spherical mirrors having radius of curvature equal to 2.9 m), while the

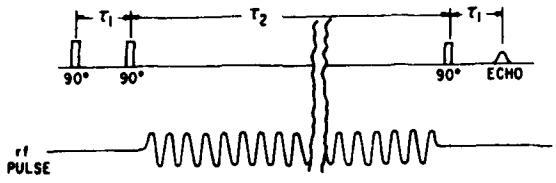

FIG. 1. Laser and radio-frequency excitation pulses for PENDOR experiment.

other was combined and made collinear with the output of the second laser by beam combiner BC1. The delayed beam from the White cell was then combined with the other two beams at BC2. The temporal separation between laser pulses 1 and 2 was adjusted to be 130 nsec, and the separation between pulses 2 and 3 was adjusted to be either 20 or 40 μsec. The three collinear pulses were focused to a 100-μm-diameter spot in the sample by a 20-cm-focal-length lens. The sample, whose Pr^{3+} concentration was 1.0 at. wt.%, had a thickness of 2.5 mm, and was mounted in a cryostat that was maintained at a temperature of 2.5 K. The c axis of the crystal was perpendicular to its optically buffed surface, and parallel to the direction of propagation of the laser pulses. The rf pulse was applied to the sample by means of a 1-μH, 4-mm-diameter coil consisting of 10 turns of 30-gauge copper wire wound about the sample in such a way that the oscillating rf field was parallel to the crystal c axis. The coil was energized by a broadband 3-W amplifier (ENI model 300 L) driven by a Hewlett-Packard frequency synthesizer whose output

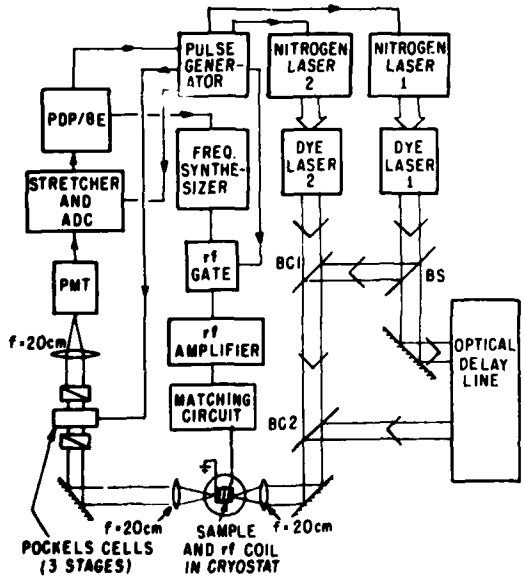

FIG. 2. Experimental arrangement for PENDOR measurements. See text for detailed explanation.

was gated on between the second and third laser pulses. The rf gating circuit was triggered by a multipulse-generator unit that was interfaced to a PDP 8/e minicomputer, making it possible to gate the rf field on and off under program control. The output of the frequency synthesizer was also controlled by the PDP 8/e. To enhance the rf field at the sample, an impedance matching circuit was inserted between the rf amplifier and the coil at the sample. After passing through the sample, the laser beams were recollimated by another 20-cm-focal-length lens and then directed into an RCA-C31034 photomultiplier tube (PMT). The three excitation pulses were prevented from saturating the PMT by three stages of crossed polarizers and Pockels cells that were pulsed open about 30 nsec before the arrival time of the stimulated echo. The output of the PMT was amplified and fed into a gated stretcher and then directed to an analog-to-digital converter. To eliminate the effects of long-term drift in the echo signal due to changes in laser intensity or optical alignment, the rf field was alternately gated on and off, with the computer separately averaging the stimulated photon echo intensity for the two cases. The average was taken over 200 shots. The value of $(I_{rf}-I_{nrf})/I_{nrf}$, where $I_{rf}(I_{nrf})$ stands for the echo intensity with (without) the rf field gated on, is then printed out by the computer as a function of rf frequency. The Q of our matching circuit was ~ 100 and we had to adjust the matching circuit capacitors whenever the frequency was changed.

Figure 3 shows the percentage decrease in the stimulated photon echo intensity as a function of the applied rf frequency. The dips at 3.7 and 4.65 MHz correspond to the energy splittings in the excited $^1D_2$ state, and agree well with Erickson's reported values of 3.7 and 4.7 MHz.[4] Our measured linewidths of 350 kHz [full width at half maximum (FWHM)] for the two resonances are, however, larger than the 200 $\pm$50-kHz linewidth that he reported.[8] This discrep-

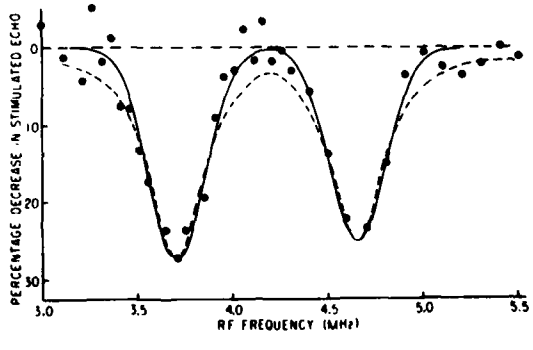

FIG. 3. PENDOR resonance curve, showing $^1D_2$ excited state splittings in $LaF_3:Pr^{3+}$.

ancy can perhaps be explained by the suppositon that the 200-kHz linewidth he inferred is a consequence of his assuming a Lorentzian line shape for deconvolving the observed line shape from the laser line shape. For a Gaussian line shape, the inferred linewidth can be a factor of 2 larger.[9] In Fig. 3 the solid and dotted lines are Gaussian and Lorentzian fits, respectively, to the data points with a (FWHM) linewidth of 350 kHz. The quality of our data prevents our preferring one over the other, but since a large part of the inhomogeneity of the nuclear hyperfine levels is due to the perturbing effects of eleven ^{19}F neighbors,[10] one would expect the linewidth to be Gaussian rather than Lorentzian.

Previous work which Fourier analyzed photon-echo-modulation data for the $^3H_4$-$^3P_0$ transition[1] has shown that the inhomogeneous linewidth of the nuclear transitions in the $^3P_0$ state is approximately 20 kHz, while the inhomogenous linewidth of the $^3H_4$ ground state is approximately 200 kHz. For the $^3P_0$ state, $J=0$, and the linewidth is due primarily to the static dipolar and quadrupolar interactions of the ^{141}Pr nucleus with the neighboring ^{19}F nuclei and the electric field gradient at the ^{141}Pr site, respectively. For the $^3H_4$ state, $J=4$ and the close spacing of the crystal-field-split levels of the $^3H_4$ multiplet gives rise to an enhanced nuclear moment that interacts strongly with the surrounding nuclear neighbors and leads to an increased linewidth. In like manner the $^1D_2$ multiplet levels are broadened beyond the 20-kHz width of the $^3P_0$ state. According to a second moment calculation, the contribution to the inhomogeneous linewidth from the unenhanced Pr-F nuclear dipolar interaction is 13 kHz.[11] When we take into account the experimentally determined enhanced nuclear gyromagnetic ratio of $\gamma/2\pi = 10$ kHz/G for the $^1D_2$ state[11,12] we obtain an inhomogeneous linewidth of approximately 120 kHz. The contribution from other sources such as lifetime broadening (~ 600 Hz) and phonon processes (~ 800 Hz) (Ref. 4) are negligible. Since we typically used rf pulses 20-μsec long, the contribution to the linewidth due to the finite duration of the rf field is 8 kHz. The remaining 220 kHz of the measured 350-kHz linewidth that must be accounted for is possibly due to rf power broadening.

In conclusion, using a photon-echo nuclear-double-resonance technique, we have shown that the nuclear splittings in the $^1D_2$ state, as inferred by Erickson from his saturated-and-enhanced-absorption study of the $^3H_4$-$^1D_2$ transition in LaF_3:Pr^{3+}, are correct.

ACKNOWLEDGMENTS

This work was supported by the Joint Services Electronics Program (U.S. Army, U. S. Navy, and U.S. Air Force) under Contract No. DAAG29-79-C-0079, and by the National Science Foundation and the Army Research Office under NSF Grant No. DMR80-06966.

---

*Present address: IBM Research Laboratory, San Jose, Calif. 95193.

[1] Y. C. Chen, K. Chiang, and S. R. Hartmann, Phys. Rev. B 21, 40 (1980).

[2] Y. C. Chen, K. Chiang, and S. R. Hartmann, Opt. Commun. 29, 269 (1978).

[3] K. Chiang, E. A. Whittaker, and S. R. Hartmann (unpublished).

[4] L. E. Erickson, Phys. Rev. B 16, 4731 (1977).

[5] It also seemed something of a coincidence that the excited-state splittings of 3.7 and 4.7 MHz should almost sum to the well-verified 8.47-MHz ground-state splitting. See Refs. 3, 4, and 9.

[6] P. Hu, R. Leigh, and S. R. Hartmann, Phys. Lett. 40A, 164 (1972).

[7] P. F. Liao, P. Hu, R. Leigh, and S. R. Hartmann, Phys. Rev. A 9, 332 (1974).

[8] Subsequent measurements of the $^1D_2$-$^3H_4$ homogeneous optical width of 40 kHz [see R. M. Macfarlane, R. M. Shelby, and R. L. Shoemaker, Phys. Rev. Lett. 43, 1726 (1979)] show Erickson's linewidth to be dominated by the inhomogeneous nuclear width and therefore a comparison between his measurement and ours is valid in this case.

[9] A. Yamagishi and A. Szabo, Opt. Lett. 2, 160 (1978).

[10] R. M. Shelby, C. S. Yannoni, and R. M. Macfarlane, Phys. Rev. Lett. 41, 1739 (1978).

[11] Y. C. Chen, K. Chiang, and S. R. Hartmann, Opt. Commun. 29, 181 (1979).

[12] R. Devoe (private communication).

PHYSICAL REVIEW B VOLUME 26, NUMBER 7 1 OCTOBER 1982

Hyperfine structure of the $^1D_2$-$^3H_4$ levels of Pr^{3+}:LaF_3 with the use of photon echo modulation spectroscopy

E. A. Whittaker and S. R. Hartmann
Columbia Radiation Laboratory, Department of Physics, Columbia University, New York, New York 10027
(Received 1 March 1982)

We have performed a photon echo modulation measurement of the $^1D_2$-$^3H_4$ levels of Pr^{3+}:LaF_3. This time-domain method yields a precise determination of the $^1D_2$ excited-state hyperfine splittings and linewidths. New information on the relative orientation of the principal axes of the excited- and ground-state hyperfine Hamiltonians is presented.

In this paper we present the results of a photon echo modulation measurement of the hyperfine structure and line-broadening character of the lowest crystal-field-split levels of the $^1D_2$-$^3H_4$ transition in Pr^{3+}:LaF_3. These electronic singlets are each split into three pairs of doublets by the second-order hyperfine and electric quadrupole interactions.[1,2] The splittings are of the order of 10 MHz. Both the nuclear and the optical transitions of this system are broadened by the magnetic interaction of the Pr and F nuclei.[3] While the nuclear magnetic interactions are enhanced by second-order electronic coupling,[4] these interactions are still weak, and the optical homogeneous linewidth is one of the narrowest ever seen in a solid.[5] The spectra described in this paper have been measured previously by enhanced and saturated absorption,[2] photon echo nuclear double resonance,[6] and nonmodulated photon echo.[5] Our result, however, represents the first measurement of the splittings and linewidths of this transition carried out entirely in the time domain and provides new information on the relative orientation of the principal axes systems of the ground $^3H_4$ and excited $^1D_2$ hyperfine Hamiltonians.

Hyperfine spectroscopy using photon echo modulation has been described completely by Chen *et al.*[7] who studied the $^3P_0$-$^3H_4$ transition in Pr^{3+}:LaF_3. We summarize here the basic method and some improvements we have made. Two laser pulses, resonant with the $^1D_2$-$^3H_4$ transition and separated in time by τ, are incident upon a 10-mm-long sample, cooled to 2.5 K. This preparation gives rise to a rephased dipole moment at time 2τ after the first pulse, given by

$$P(2\tau)=\vec{P}(0)(2I+1)^{-1}\sum_{\alpha,\beta,\gamma,\epsilon=1}^{2I+1}(W)_{\alpha\beta}(W^{-1})_{\beta\gamma}(W)_{\gamma\epsilon}(W^{-1})_{\epsilon\alpha}\exp[-(\Omega^{(e)}_{\alpha\gamma}+\Omega^{(g)}_{\beta\epsilon})\tau]$$
$$\times\cos[(\omega^{(e)}_{\alpha\gamma}-\omega^{(g)}_{\beta\epsilon})\tau]\exp(-2\tau/T_2)\,, \quad (1)$$

where the notation is that of Ref. 7. The essential features of this formula are its dependence on the W matrices, which carry information on the relative orientation of the ground- and excited-state hyperfine Hamiltonians, the nuclear hyperfine transition linewidths Ω, and the nuclear hyperfine transition frequencies ω. The measured echo intensity is the square of this amplitude and will contain beats from both the fundamental hyperfine frequencies and their harmonics.

The experimental method utilizes two electronically triggered nitrogen laser-pumped dye lasers. The 1-GHz wide, kilowatt pulses are made collinear and focused to a 100-μm spot on the 0.1 wt. % sample of Pr^{3+}:LaF_3. The echo signal is detected through a Pockels cell shutter by an RCA C31034 photomultiplier tube. A PDP8/e computer is used to control and sweep the laser pulse separation through a desired range, and to integrate and digitize the echo intensity for each laser shot. To eliminate the effects of a remnant (10–20)-nsec laser pulse separation jitter, a computer-read ORTEC 457 time-to-pulse-height converter is used to put each echo shot into the appropriate 5-nsec-wide bin in the computer memory. To compensate for laser amplitude drift and to facilitate averaging data from many sweeps, the computer was made to periodically record the echo intensity at a fixed

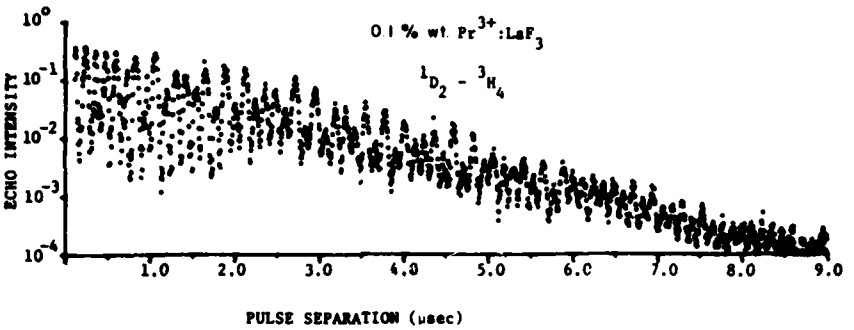

FIG. 1. Photon echo intensity vs laser pulse separation for the $^1D_2$-$^3H_4$ transition of 0.1 wt. % Pr^{3+}:LaF_3.

reference time ($\tau = 600$ nsec). Figure 1 shows the average echo intensity versus pulse separation. Each point is the average of at least 100 shots and the data shown represent the average of about 30 separate runs. A given run covers about 1 μsec of data. To eliminate the effect of optical pumping in the ground state[1] (which for this method produces an artifact known as long-lived stimulated echo[8]), the 16.7-MHz ground-state hyperfine resonance is saturated with rf energy between laser shots.

The overall decay of the echo in Fig. 1 reflects a homogeneous optical linewidth of 72 kHz (corresponding to $T_2 = 4.4$ μsec for a Lorentzian line shape), consistent with several other recent measurements.[5,9] More information may be extracted from this data by examining its Fourier transform, shown in Fig. 2. Before Fourier transformation, the data of Fig. 1 were multiplied by a factor $\exp(+4\tau/T_2)$ so that the resonance linewidths of Fig. 2 do not include the overall optical decay linewidth. The three strong resonances at 3.72, 4.79, and 8.51 MHz are the hyperfine frequencies of the $^1D_2$ excited states. Weaker resonances (note that beyond 10 MHz the vertical scale is 100 times more sensitive) at 12.24, 13.26, and 17.04 MHz are from mixing of the first three strong resonances. There are also ground-state resonances at 8.48, 16.7, and 25.14 MHz but the 8.48-MHz line is masked by the stronger 8.51-MHz excited-state line, and the 16.7-MHz line appears to be split. We believe that this splitting is an unanticipated effect of the 16.7-MHz rf energy used to eliminate long-lived stimulated echo, and probably arises because for pulse separations greater than 3 μsec the rf energy was inadvertently allowed to overlap the echo pulse sequence.

The resonance widths reflect the total (inhomogeneous and homogeneous) nuclear linewidths of the various hyperfine transitions. Previous measurements[1,7] have shown the ground-state widths to be about 200 kHz. This width is mostly inhomogeneous and arises from the interaction of the enhanced ground-state ^{141}Pr nuclear moment of 11.5 kHz/G (Ref. 1) and the surrounding distribution of static ^{19}F nuclear moments. Macfarlane and Shelby[10] have measured the g tensor for the $^1D_2$ state and found the enhancement to be roughly 5 times less than in the ground state. This would lead one to expect a much narrower linewidth for the nuclear transitions in the $^1D_2$ state and our measurement, while very nearly resolution limited by the overall echo-decay envelope, places a new upper limit of 30 kHz (full width at half maximum) for the 8.51-MHz linewidth, consistent with this expectation. The 3.72- and 4.79-MHz linewidths are

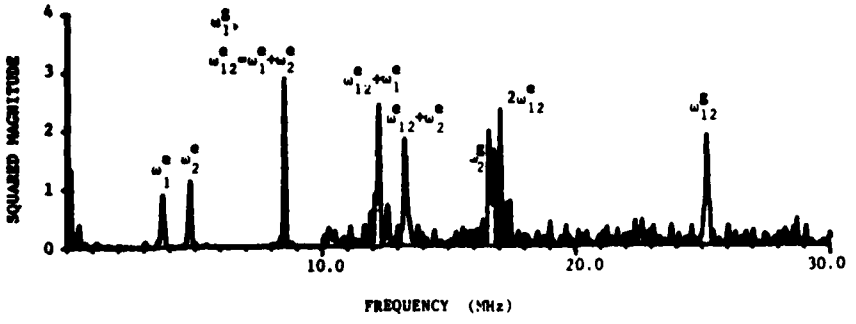

FIG. 2. Squared magnitude of the Fourier transform of the data in Fig. 1. The data were first multiplied by $\exp(\tau/1.2$ μsec). The vertical scale is 100 times more sensitive for frequencies beyond 10 MHz.

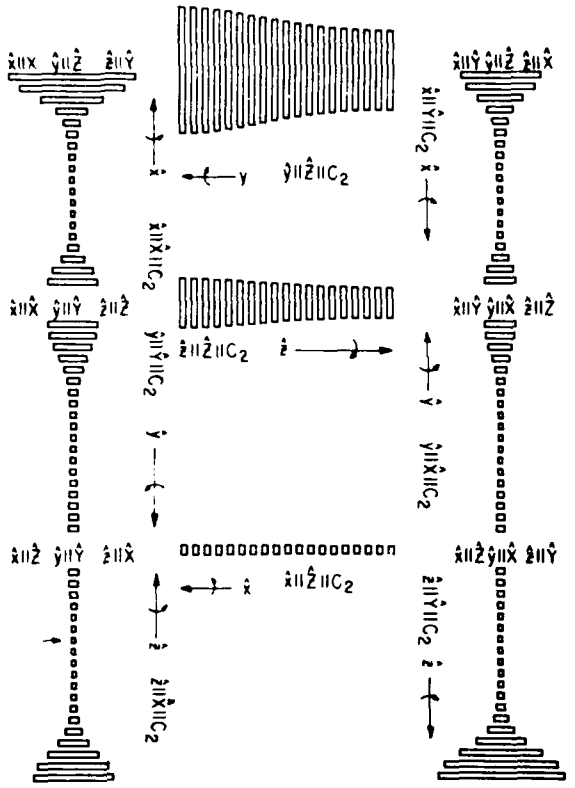

FIG. 3. Map of minimum mean-square deviation between echo data and theoretical curve of Eq. (1), as a function of the relative orientation of the ground- and excited-state hyperfine Hamiltonians. The arrow at the lower left points to the coordinate with the best fit.

somewhat larger, at 70 and 60 kHz, respectively. The results for the $^1D_2$ excited-state parameters are summarized in Table I.

The expression for echo modulation is given analytically by Eq. (1). Once Fourier analysis has given the splittings and linewidths, the only remaining parameters define the relative orientation of the ground- and excited-state effective hyperfine Hamiltonian principal axes. This Hamiltonian may be written

$$H_{g(e)}=\nu_{g(e)}\left[I^2_{z(Z)}+\frac{\eta_{g(e)}}{3}(I^2_{x(X)}-I^2_{y(Y)})\right]. \tag{2}$$

The upper and lower case subscripts emphasize that the ground (g) and excited (e) state principal axes need not be the same, although Neumann's principle requires that they have at least one common axis parallel to the local C_2 symmetry axis. This constraint significantly reduces the number of possible orientations, and we may represent these possibilities on a two-dimensional map.[7] The coordinates of such a map give the particular choice of common axes, and the angle θ through which one set of axes is rotated with respect to the other set about the common axis. Since the Hamiltonian in Eq. (2) is insensitive to the sign of the coordinates, an orientation of, for example, $\hat{x}||\hat{X}$ is equivalent to $\hat{x}||-\hat{X}$. We have calculated the echo modulation curve, Eq. (1), in increments of five degrees in the rotation angle θ. Figure 3 presents a map where for each orientation coordinate a box is drawn whose width is proportional to the minimum mean-square deviation between our data and the calculated curves. Only the first microsecond of data was used in the fitting procedure for Fig. 3. Beyond 1 μsec, the data are dominated by the excited-state hyperfine splittings due to the relative linewidths of ground- and excited-state levels and including these data in the fit considerably reduces the selectivity of the map.

TABLE I. Values for the $^1D_2$ excited-state hyperfine frequencies and nuclear linewidths obtained from the Fourier transform of the data in Fig. 1. The linewidths have been corrected for the effect of the finite truncation interval (Ref. 7).

Resonance	Frequency	Full width at half maximum
ω_1^e	3.72±0.02 MHz	70±20 kHz
ω_2^e	4.79±0.02 MHz	60±20 kHz
ω_{12}^e	8.51±0.02 MHz	30±30 kHz

Figure 4 shows in expanded scale the first three microseconds of (a) our data and (b) the theoretical curve calculated from Eq. (1) using the orientation coordinate giving the best fit to the data (as indicated by an arrow in the lower left of Fig. 3). The curves of Fig. 4, having been multiplied by the factor $\exp(+4\tau/T_2)$, do not include the effect of the overall optical linewidth. The slight rise in the echo peaks of Fig. 4(a) is an artifact in the data due to detector saturation at short pulse separation. This saturation may also be seen in Fig. 1, where the initial envelope decay is somewhat slower than the corresponding decay for the rest of the data. This artifact introduces some uncertainty in the estimate of optical linewidth but seems to have negligible effect on the Fourier transform and overall fit since another data set with smaller overall signal-to-noise ratio, but without the saturation, gives similar results to those presented here.

The map in Fig. 3 shows a high degree of symmetry and concommitant lack of selectivity for

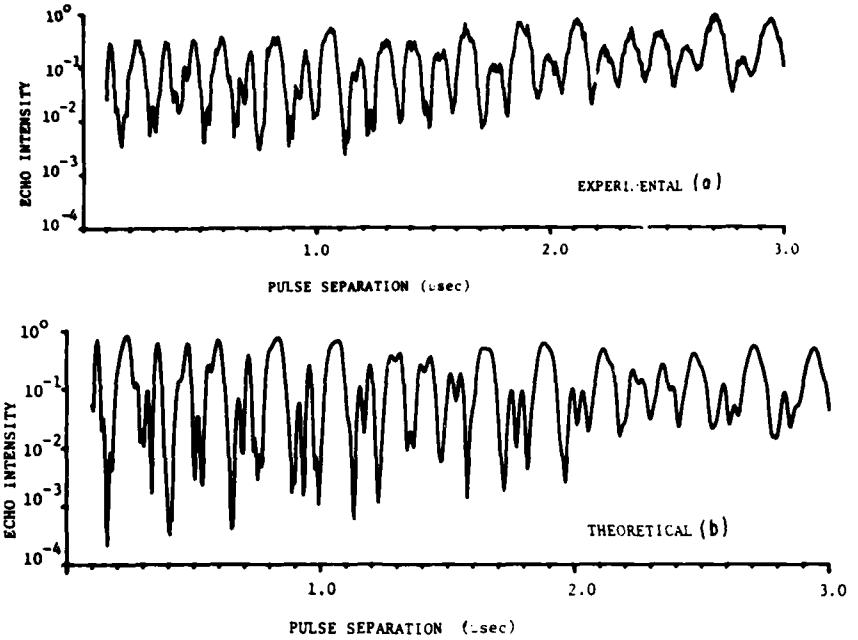

FIG. 4. Comparison of the first three microseconds of data (a) and the theoretical curve (b) for the orientation giving the smallest mean-square deviation.

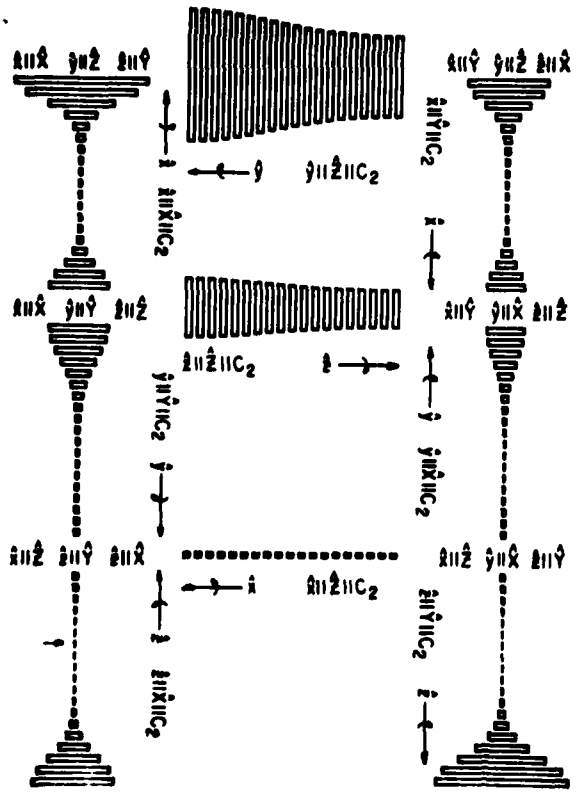

FIG. 5. Map of mean-square deviation between the theoretically calculated data of Fig. 4(b) and the theoretical curve of Eq. (1). Notice the similarity to Fig. 3.

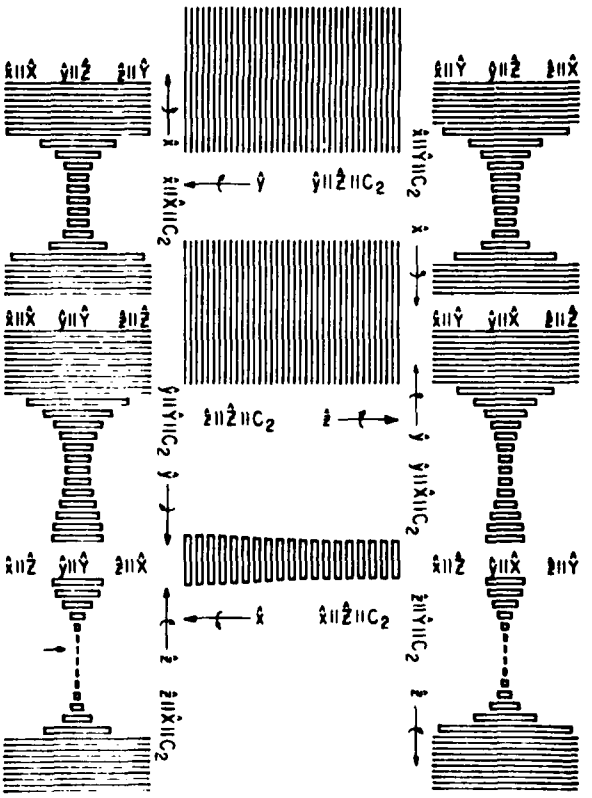

FIG. 6. Map of Fig. 5 with the scale for the box width expanded by a factor of 10.

determining the orientation parameter. To explore the extent to which this symmetry is intrinsic to the form of Eq. (1), we have substituted for the data used to calculate the map of Fig. 3 the values of the theoretical curve corresponding to Fig. 4(b), producing the map shown in Fig. 5. The scale in Fig. 5 was chosen to make the box corresponding to the coordinate with the worst fit in Fig. 5 approximately the same size as the box with the worst fit in Fig. 3. It is apparent that the high degree of symmetry persists. To estimate the extent to which our signal-to-noise ratio would need to improve and so allow us to select one orientation with certainty, we replotted Fig. 5 with the box width scale expanded by a factor of 10, as shown in Fig. 6. It appears that an improvement in the signal-to-noise ratio by a factor of 10 or 20 would have made possible a more definitive statement about the orientation. This improvement will probably come from the use of frequency- and amplitude-stabilized dye lasers. Frequency jitter in particular causes considerable fluctuation in echo intensity, presently averaged by the data-taking system, and such averaging tends to wash out some of the fine details of the modulation pattern. Despite the high symmetry, we can draw a number of conclusions about the relative orientation. All configurations with all axes parallel are ruled out, as are those with the excited-state $\hat{Z}$ axis parallel to C_2. These conclusions are similar to the measurement by Chen *et al.*[7] of the relative orientation of the $^3H_4$ and $^3P_0$ states. Since the g tensor is nearly isotropic in the $^1D_2$ state[10] and absent completely in the $^3P_0$ state, the relative orientation parameter must be primarily determined by the relative orientation of the pure quadrupole tensor with respect to the ground-state hyperfine tensor.

Our photon echo modulation analysis of the $^1D_2$-$^3H_4$ Pr^{3+}:LaF_3 transition hyperfine structure gives a new time-domain measurement of the splittings and linewidths which accords well with previous measurements. We also present new information on the relative orientation of the effective hyperfine Hamiltonians.

One of us (E.W.) wishes to thank Frank Abramopoulis for a useful suggestion concerning the data analysis. This work was supported by the Joint Services Electronics Program (U. S. Army, U. S. Navy, and U. S. Air Force) under Contract No. DAAG29-79-C-0079 and by the National Science Foundation and the Army Research Office under Grant No. NSF-DMR80-06966.

[1]L. E. Erickson, Opt. Commun. 21, 147 (1977).
[2]L. E. Erickson, Phys. Rev. B 16, 4731 (1977).
[3]R. G. DeVoe, A. Wokaun, S. C. Rand, and R. G. Brewer, Phys. Rev. B 23, 3125 (1981).
[4]B. Bleaney, Physica 69, 317 (1973).
[5]R. M. Macfarlane, R. M. Shelby, and R. L. Shoemaker, Phys. Rev. Lett. 43, 1726 (1979).
[6]K. Chiang, E. A. Whittaker, and S. R. Hartmann, Phys. Rev. B 23, 6142 (1981).
[7]Y. C. Chen, K. Chiang, and S. R. Hartmann, Phys. Rev. B 21, 40 (1980).
[8]Y. C. Chen, K. Chiang, and S. R. Hartmann, Opt. Commun. 29, 269 (1979). The artifact occurs because a three-pulse stimulated echo, formed by two excitation pulses of one laser shot and the second excitation pulse of the succeeding shot, occurs simultaneous with the ordinary echo signal. This effect was not compensated for in the experiment of Ref. 7 and may have distorted their result somewhat.
[9]R. G. DeVoe, A. Szabo, S. C. Rand, and R. G. Brewer, Phys. Rev. Lett. 42, 1560 (1979).
[10]R. M. Macfarlane and R. M. Shelby, Opt. Lett. 6, 96 (1981).

PHYSICAL REVIEW A VOLUME 23, NUMBER 5 MAY 1981

Propagation narrowing in the transmission of a light pulse through a spectral hole

J. H. Eberly
Department of Physics and Astronomy, University of Rochester, Rochester, New York 14627

S. R. Hartmann
Columbia Radiation Laboratory, Department of Physics, Columbia University, New York, New York 10027

A. Szabo
Division of Electrical Engineering, National Research Council of Canada, Ottawa, Canada K1AOR8

(Received 20 October 1980)

We comment on the spectral modification and temporal reshaping of a narrow-band light pulse propagating through an atomic absorber that has a still narrower spectral hole. The regime of propagation narrowing is distinguished from the regime of Beer's law.

I. INTRODUCTION

Hole burning is the term for the selective photoexcitation of atoms or molecules in a small portion of an inhomogeneously broadened optical absorption line. In this region of the line, following the photoexcitation, there will be fewer than the normal number of atoms or molecules in their ground states. A subsequent narrow-band weak probe pulse will suffer less than normal attenuation if its center frequency lies within the excitation region. The resulting absorption curve mapped out by scanning the frequency of the probe beam has a hole in it. Figure 1 shows an example. All of this is well known.[1]

In the present note we address a question that comes up when the weak probe pulse has a spectral width greater than the width of the hole, as shown in Figure 2. This question is: What is the temporal form of the transmitted pulse? The uncertainty relation $\Delta\nu\Delta\tau \geq 1$ suggests that $\Delta\tau$ increases because $\Delta\nu$ decreases, but in order to answer the question properly it turns out to be necessary to consider the propagation of the probe pulse through a finite depth of absorber. If the probe pulse is weak enough to have negligible effect on the hole, then the question can be answered analytically in closed form.

II. PROPAGATION OF WEAK OPTICAL PULSES THROUGH BROADBAND INHOMOGENEOUSLY BROADENED ABSORBERS

In the familiar two-level-atom model for an absorber,[2] transmission and absorption of light are governed by the equation

$$(\partial/\partial z + \partial/\partial ct)\mathcal{E}(t,z) = 2\pi i(\omega/c)\mathcal{P}(t,z), \qquad (1)$$

where $\mathcal{E}$ and $\mathcal{P}$ are the complex envelopes of the electric field strength and the atomic polarization density. An expression for $\mathcal{P}$ involves the off-diagonal part of the two-level atom's density

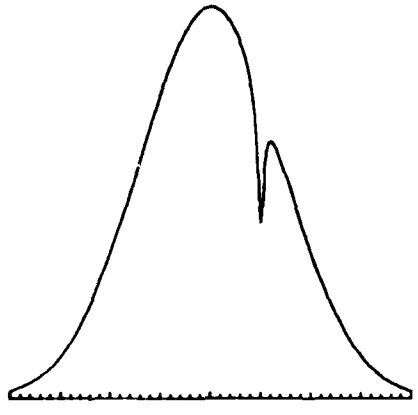

FIG. 1. A Doppler-broadened absorption line with a homogeneously broadened hole.

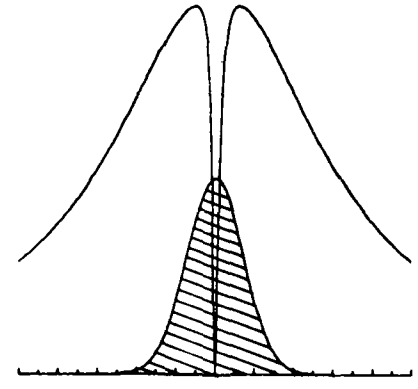

FIG. 2. The initial probe pulse spectrum (shaded) overlaid on an absorption line with a much narrower spectral hole.

matrix in the rotating wave approximation, averaged over the Doppler distribution of atomic velocities:

$$\mathcal{P}(t,z) = Nd\langle r_{12}(t,z;v)\rangle_v . \tag{2}$$

Here, N is the density of atoms and d is the magnitude of the atomic transition dipole matrix element along the direction of the electric field vector.

If, as we assume, the electric field of the probe pulse is too weak to alter the shape of the inhomogeneous line (with the hole already burned into it), then the equation obeyed by $r_{12}(t,z;v)$ is simply

$$\partial r_{12}/\partial t = -(\beta + i\Delta) r_{12} + (i/\hbar)\, d\,\mathcal{E}. \tag{3}$$

Here, $\Delta = \Delta(v)$ is the detuning between pulse frequency and the Doppler-shifted atomic resonance frequency and β is the halfwidth of the homogeneous component of the atomic absorption line. An average over Δ's is equivalent to an average over v's.

Because Eqs. (1) and (3) are linear they are trivially solved by Fourier transform methods. We define

$$\mathcal{E}(t,z) = \int e(\nu,z)\, e^{-i\nu t}\, d\nu/2\pi , \tag{4a}$$

$$r_{12}(t,z) = \int \rho(\nu,z)\, e^{-i\nu t}\, d\nu/2\pi , \tag{4b}$$

and find the equation

$$[\partial/\partial z - i\nu/c - i f(\nu) + \tfrac{1}{2} g(\nu)]\, e(\nu,z) = 0 , \tag{5}$$

where f and g are the dispersive and absorptive parts of the dipole reaction field:

$$f(\nu) = -\tfrac{1}{2} G\, \mathrm{Im}\left\langle \frac{1}{\beta + i(\Delta - \nu)} \right\rangle , \tag{6a}$$

$$\tfrac{1}{2} g(\nu) = \tfrac{1}{2} G\, \mathrm{Re}\left\langle \frac{1}{\beta + i(\Delta - \nu)} \right\rangle , \tag{6b}$$

Here, G is the primitive attenuation parameter for the problem

$$G = 4\pi N d^2 \omega/\hbar c , \tag{7}$$

and the angular brackets denote the Doppler average.

The solution to Eq. (5) is immediate:

$$e(\nu,z) = \mathcal{E}_0 e^{-1/2(\nu/\delta\nu_0)^2} e^{if(\nu)z} e^{-1/2 g(\nu)z} . \tag{8}$$

We have assumed that the incident pulse is Gaussian in time, with bandwidth $\delta\nu_0$ and temporal length $2\pi/\delta\nu_0$.

The pulse Fourier energy spectrum obviously changes with propagation:

$$|e(\nu,z)|^2 = |\mathcal{E}_0|^2 e^{-(\nu/\delta\nu_0)^2} e^{-g(\nu)z} . \tag{9}$$

However, in the usual case, when the Doppler linewidth is appreciably greater than $\delta\nu_0$, we can take $g(\nu) = g(0)$ for all significant frequencies ($|\nu| \lesssim \delta\nu_0$). Then the only significant frequency dependence is due to the Gaussian factor that came from the incident pulse. Thus the pulse retains its Gaussian shape and is simply attenuated uniformly at all frequencies according Beer's law:

$$|e(\nu,z)|^2 \cong |\mathcal{E}_0|^2 e^{-(\nu/\delta\nu_0)^2} e^{-g(0)z} . \tag{10}$$

All this is well known, and Crisp[3] has given interesting examples showing dramatic departures from the kind of behavior implied by (10) when the pulse bandwidth is much greater, rather than less, than the Doppler linewidth.

III. PROPAGATION THROUGH A SPECTRAL HOLE

With the background formulas derived in Sec. II, it is easy to take into account a narrow hole in the Doppler line. For simplicity we will take the shape of the Doppler curve, as well as the hole, to be Lorentzian. This is realistic as far as the hole is concerned and not a bad approximation for the Doppler curve because we will be concerned only with its center portion. Another simplication will be to take the centers of the spectral curves of the incident pulse, the Doppler line, and the hole all to coincide at $\nu = 0$, as shown in Fig. 2. Under these conditions the angular bracket in Eqs. (6) is to be interpreted as an average over Doppler detuning Δ with the normalized weight function

$$p(\Delta) = \frac{\beta^*}{\pi} \frac{1}{\Delta^2 + (\beta^*)^2} ,$$

where β^* is obviously now the Doppler width. Then we can evaluate the brackets in Eqs. (6) by explicit integration and find

$$f(\nu) = -\tfrac{1}{2}\alpha \left(\frac{\nu/\beta^*}{1 + (\nu/\beta^*)^2} - \frac{\nu/\beta_H}{1 + (\nu/\beta_H)^2} \right), \tag{11a}$$

$$\tfrac{1}{2} g(\nu) = \tfrac{1}{2}\alpha \left(\frac{1}{1 + (\nu/\beta^*)^2} - \frac{1}{1 + (\nu/\beta_H)^2} \right), \tag{11b}$$

where α is the normal Doppler absorption coefficient at line center:

$$\alpha = 4\pi N d^2 \omega/\hbar c\, \beta^* , \tag{12}$$

and β^* and β_H are the half-widths of the Dopper line and the hole, respectively. We are principally interested in the limits

$$\beta^* \gg \delta\nu_0 \gg \beta_H \gg \beta . \tag{13}$$

In other words, we assume the Doppler line to be much broader than any other spectral feature, and the width of the incident pulse to be much broader than the hole in the Doppler line. The

underlying homogeneous width is taken to be negligibly small compared to all the other widths. These conditions are qualitatively met by the curves in Fig. 2.

Given relation (13), there are two distinct regions of the spectrum:

(a) The region of *propagation narrowing*, where $\nu \lesssim \beta_H$.

(b) The region of *Beer's law*, where $\nu \gg \beta_H$.

We have discussed region (b) briefly in Sec. II. Region (a) is characterized by a simple approximate expression for $g(\nu)$:

$$g(\nu) \simeq \alpha(\nu/\beta_H)^2. \tag{14}$$

Thus, in region (a) we have

$$|e(\nu,z)|^2 = |\mathcal{E}_0|^2 e^{-\nu^2/[\delta\nu(z)]^2}, \tag{15}$$

where

$$\delta\nu(z) = \beta_H/[\alpha z + (\beta_H/\delta\nu_0)^2]^{1/2}. \tag{16}$$

That is, in the region of propagation narrowing the spectrum is Gaussian but with a variable width. Note that at $\alpha z = 0$ the width is equal to the initial pulse width $\delta\nu_0$ and only becomes smaller due to propagation. The decrease can, however, be rapid because $\beta_H/\delta\nu_0$ can be much less than unity. The threshold for propagation narrowing occurs at $\alpha z \approx (\beta_H/\delta\nu_0)^2$.

In the region of Beer's law the spectrum is also Gaussian, but with width $\delta\nu_0$, independent of αz.

To interpolate between regions (a) and (b) requires the full expression (11b) for $g(\nu)$. In Fig. 3 we show the full $|e(\nu,z)|^2$ as a function of ν for several values of αz, given the ratios $\beta^*/\delta\nu_0 = \sqrt{10}$ and $\beta_H/\delta\nu_0 = 1/10$. The two distinct Gaussians appropriate to spectral regions (a) and (b) are evident. Figure 4 shows the effect of the hole

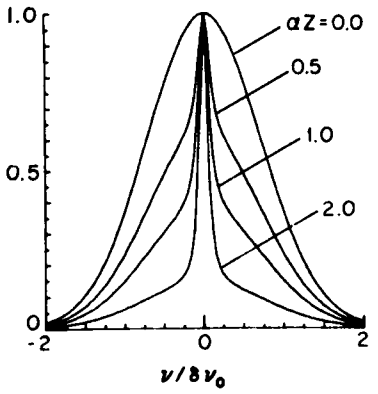

FIG. 3. The spectrum of the probe pulse $|e(\nu,z)|^2$ at a succession of propagation depths $\alpha z = 0.0$, 0.5, 1.0, and 2.0. The horizontal axis is in units of $\delta\nu_0$.

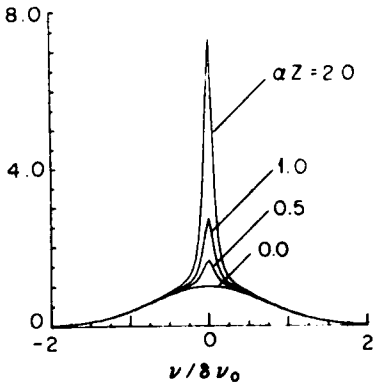

FIG. 4. The spectrum of the probe pulse, as in Fig. 3, except that the normal component of absorption has been removed.

alone by plotting $|e(\nu,z)|^2$ without the first term of $g(\nu)$. In effect, Fig. 4 shows that the relative importance of the hole grows with propagation, but, as expected, only near line center. The broad base of all of the curves is simply $\exp[-(\nu/\delta\nu_0)^2]$.

IV. TIME-DEPENDENT FEATURES

The exact expressions obtained in Sec. III for $|e(\nu,z)|^2$, as well as the approximate relations valid in the regions of propagation narrowing and Beer's law, permit good qualitative estimates of the time dependence of the transmitted pulse. However, $|e(\nu,z)|^2$ does not provide everything, because the consequences of $f(\nu)$ are not included. In this section we present the results of numerical computation of the Fourier transform (4a), thereby giving the full space-time behavior of $\mathcal{E}(t,z)$.

Figure 5 shows the temporal behavior of the transmitted pulse after propagation to $\alpha z = 2$. A clear departure from the Gaussian shape of the

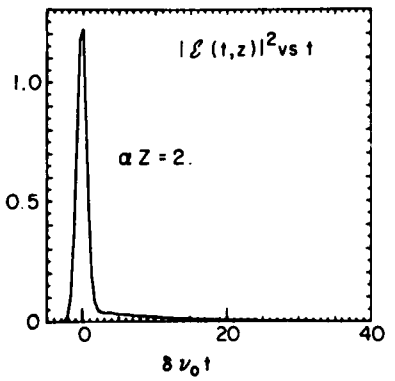

FIG. 5. The probe pulse intensity $|\mathcal{E}(t,z)|^2$ in arbitrary units as a function of time, after propagating two absorption depths into the medium. The horizontal axis is in units of $(\delta\nu_0)^{-1}$.

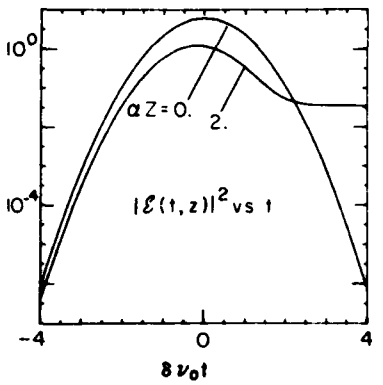

FIG. 6. The probe pulse intensity $|\mathcal{E}(t,z)|^2$ as a function of time at two different spatial positions, $\alpha z = 0$ and 2. The vertical axis is logarithmic, but to the same scale as in Fig. 5, and the units of time are $(\delta\nu_0)^{-1}$.

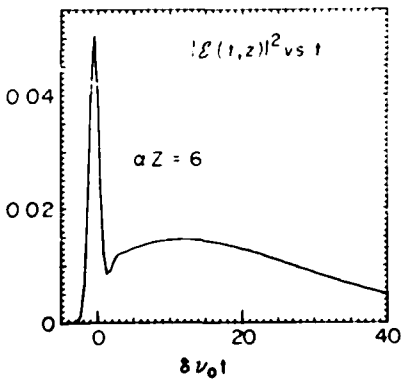

FIG. 7. The probe pulse intensity $|\mathcal{E}(t,z)|^2$ as a function of time after propagating six absorption depths into the medium. The vertical axis is to the same scale as Fig. 5, and the units of time are $(\delta\nu_0)^{-1}$.

input pulse is evident in the trailing portions of the transmitted pulse. In Fig. 6 we show the data of Fig. 5 again, but with the $z = 0$ curve added for comparison. At $\delta\nu_0 t \simeq 2$ the trailing edge of the transmitted pulse becomes stronger than the tail of the incident pulse, although it is two orders of magnitude weaker than the incident pulse peak.

Finally, Fig. 7 shows the transmitted pulse at $\alpha z = 6$. It is seen that the bulk of the pulse energy is now in the long tail, and one can begin to say that a single frequency-time uncertainty relation again describes the pulse reasonably well. The temporal width of the tail is roughly $\sqrt{3}$ times the width shown in Fig. 5, in accord with (16) since $(\beta_H/\delta\nu_0)^2$ is negligible. Moreover, we note that the resonant interaction of pulse and atoms, during the pulse transmission, is fully coherent in our model. This is responsible for the slight interference minimum that occurs between the two components of the pulse.

V. DISCUSSION

The spectral and temporal changes predicted by solution (8) are illustrated in the figures. They are a consequence of purely linear dispersion theory and are novel only in the sense that classic discussions[4] of light propagation in dispersive media do not appear to have included treatments either of purely inhomogeneous line broadening or of lines with holes in them. Experimental observations of the predicted peak delay and pulse lenghtening do not appear to have been reported either.

Another view of these results is obtained by regarding our model of an absorption line with a hole as a continuous-band interference filter. In one sense it is a pure interference filter; no energy loss mechanisms are included in the model. However, conversion of pulse energy into loss-free atomic dipole oscillations all across the Doppler line will nevertheless lead to pulse decay, and it is more realistic to speak of an interference filter, as opposed to an absorption filter, when the effect of $f(\nu)$ is much more important than that of $g(\nu)$. Formulas (11) show that for $\nu \ll \beta_H$ this condition is well satisfied:

$$f(\nu) \simeq \tfrac{1}{2}\,\alpha\nu/\beta_H\,, \tag{17a}$$

$$\tfrac{1}{2}\,g(\nu) \simeq \tfrac{1}{2}\,\alpha(\nu/\beta_H)^2\,. \tag{17b}$$

This is a consequence of the hole in the line, of course. For a normal line without a hole, one has $g \gg f$ for all frequencies near the center.

Finally, because of the linearity of the model, it is also possible to treat the pulse as if it were interacting with two entirely separate groups of atoms. The first group comprises the usual dipole oscillators in the full Doppler line, and the second group is a set of "negative" oscillators occupying a region of width β_H at line center. The negative oscillators emit rather than absorb light. It is the emission of the "negative" oscillators that causes the growth, with increasing propagation distance, of the peaks of the curves in Fig. 4. In this view of the model it is the interference between the positive and negative oscillators at line center that causes the pulse lengthening. In classical theory the negative dipoles can never be more "negative" than the real dipoles are "positive," because they are designed only to cancel the real dipoles in a certain spectral region. In the quantum theory the negative atoms are not so severely restricted. For example, the hole has been constructed in our treatment so that $g(0) = 0$. That is, we have assumed the absence of absorbing dipoles at line center. How-

ever, the original preparation of the hole could have been arranged to include a degree of atomic inversion at line center. In this case $g(0) < 0$, and gain rather than loss would be expected. The "negative" oscillators in the model would then more than cancel the positive ones. We will not explore this case.

ACKNOWLEDGMENTS

This research was partially supported by the Department of Energy, Contract No. DE-AC03-76DP01118, the Joint Services Electronics Program, Contract No. DAAG29-79-C-0079, the National Research Council of Canada, the National Science Foundation and Army Research Office, Grant No. NSF-DMR80-06966, and the Office of Naval Research, Contract No. N00014-79-0666. We are grateful to J. J. Yeh and B. J. Herman for assistance with the numerical integration required for Figs. 5–7, and we acknowledge conversations with M. A. Johnson, B. W. Shore, S. Stenholm, A. Szöke, and J. J. Yeh.

---

[1]See, for example, discussions in A. Yariv, *Quantum Electronics* (Wiley, New York, 1967), Chap. 8; M. Sargent III, M. O. Scully, and W. E. Lamb, Jr., *Laser Physics* (Addison-Wesley, Reading, Mass., 1974), Chap. 10; and L. Allen and J. H. Eberly, *Optical Resonance and Two-Level Atoms* (Wiley, New York, 1975), Chap. 6.

[2]We follow the conventions of L. Allen and J. H. Eberly, see Ref. 1.

[3]M. D. Crisp, Phys. Rev. A 1, 1604 (1970). See also Ref. 2, Sec. 1.8.

[4]A. Sommerfeld, *Optics* (Academic, New York, 1972); L. Brillouin, *Wave Propagation and Group Velocity* (Academic, New York, 1960).

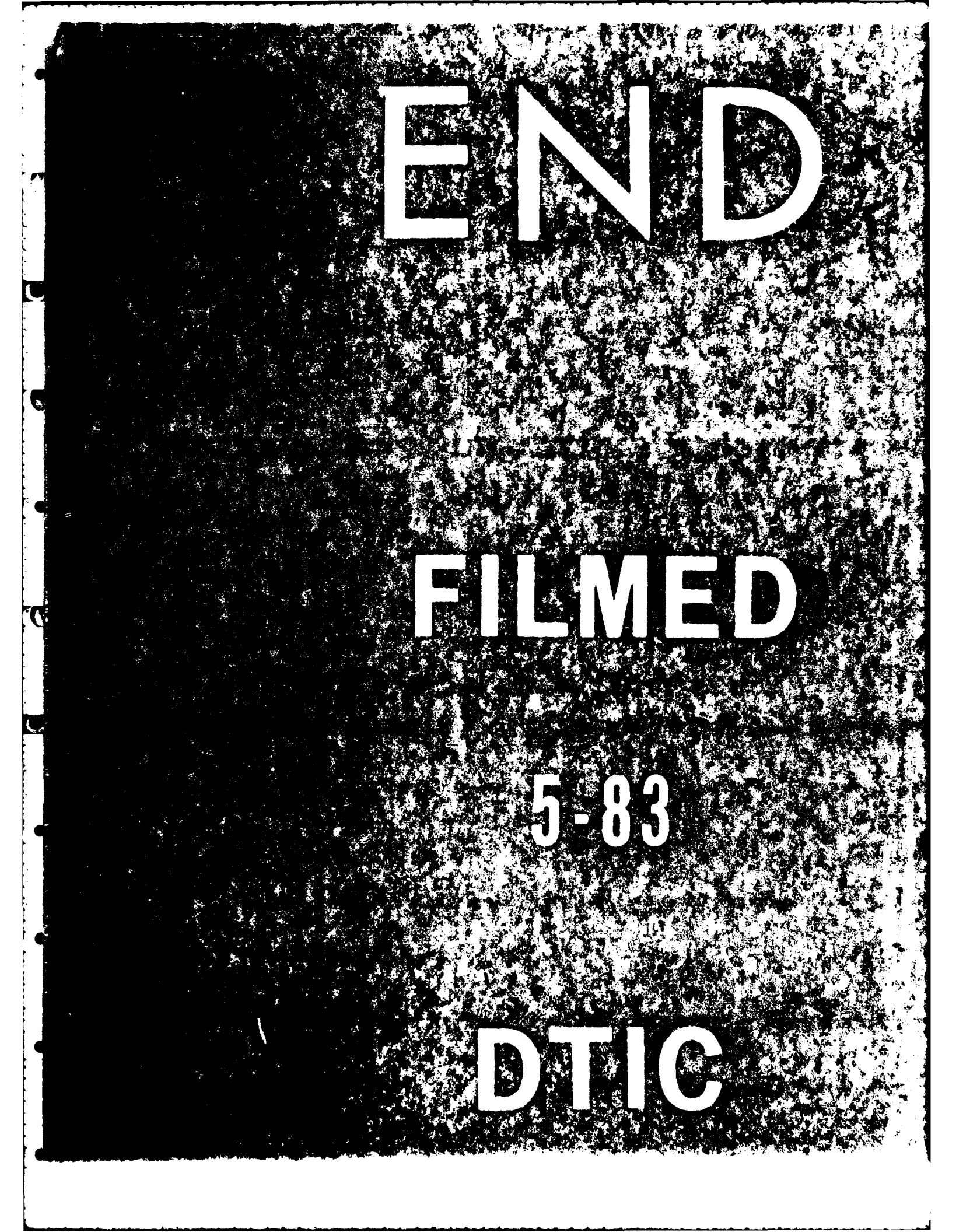
END
FILMED
5-83
DTIC